Marine Pollution Bulletin 161 (2020) 111685

Contents lists available at ScienceDirect

Marine Pollution Bulletin

journal homepage: www.elsevier.com/locate/marpolbul

Simulating particle organic matter dispersal beneath Atlantic salmon fish farms using different resuspension approaches

M.A. Carvajalino-Fernández[a,b,*], P.N. Sævik[a], I.A. Johnsen[a], J. Albretsen[a], N.B. Keeley[a]

[a] Institute of Marine Research, Postboks 1870 Nordnes, 5817 Bergen, Norway
[b] Geophysical Institute, University of Bergen, Allegaten 70, 5020 Bergen, Norway

ARTICLE INFO

Keywords:
Aquaculture
Resuspension
Parametrization
Lagrangian model
Substrate

ABSTRACT

An accurate representation of the particle organic matter (POM) footprint is necessary in order to effectively predict impacts upon benthic communities and the risk of excessive organic enrichment beneath aquaculture sea-cages. Consequently, bottom-related processes such as particle resuspension must be adequately parametrized and evaluated in the available numerical models. We implemented two approaches to model POM resuspension in a Lagrangian particle tracking model and compared their influence on footprint extension and gradients of depositional flux against a no-resuspension scenario. We performed simulations in both exposed and protected aquaculture locations, and at different stages of the Atlantic Salmon (*Salmo salar*) production cycle in Norway. Our results indicate that the use of sediment-dependent thresholds for resuspension has the potential to regulate the high levels of erosion produced when selecting a low critical value in constant-threshold approaches, particularly in dynamic environments with mixed sediment types.

1. Introduction

Open cage finfish aquaculture is associated with a broad spectrum of environmental impacts, ranging from disease transference and genetic interactions between reared and wild organisms to direct and indirect impact of fish farm wastes on the surrounding benthic ecosystems (Forrest et al., 2007; Taranger et al., 2014; Grefsrud et al., 2018). Fish farm waste comprise particulate and dissolved fractions of both organic and inorganic effluents, including but not limited to waste feed, faeces and other metabolic by-products produced during the organism's lifecycle. The particulate fraction of the waste (Particulate Organic Matter or POM hereafter) is considered the largest source of impact upon the neighboring benthic communities at aquaculture sites, with up to 70–80% in the form of faecal material (Cubillo et al., 2016; Riera et al., 2017).

POM is emitted in very large quantities. For example, large-capacity farms situated along the Norwegian coastline can discharge as much as 10 tons of fish faeces per day to the marine environment (Keeley et al., 2019); the majority of which is observed to be strongly concentrated in the first hundreds of meters around the farm. POM contains large amounts of carbon, nitrogen and phosphorus, making it an important precursor for organic enrichment of the benthic habitats, carrying the potential to generate anoxic or even azoic conditions in the close proximity to the farm (Brooks et al., 2002; Hall-Spencer and Bamber, 2007; Keeley et al., 2012). Moreover, this type of waste can be associated with a suite of potentially toxic contaminants, principally copper and zinc (Brooks and Mahnken, 2003; Dean et al., 2007; Macleod et al., 2014), but also historically, antibiotics and other feed-administered therapeutants (Burridge et al., 2010) which can pose a threat to marine life should they accumulate and become sufficiently concentrated.

The POM accumulation at a given aquaculture location, and consequently the level of benthic enrichment, depends strongly on local hydrodynamics promoting material transport, especially those processes occurring in close proximity to the seabed. Conventional particle dispersion theory and numerous studies around non-dispersive farms, i.e. those not exposed to strong currents or direct influence from open ocean conditions, describe a clear organic enrichment gradient that is severely impacted beneath the farm and out to ca. 100 m away and then grades progressively to natural conditions within ca. 300 m (Kutti et al., 2007; Borja et al., 2009; Keeley et al., 2013). In this situation, POM undergoes an initial settling process with a dominating vertical component due to the high settling velocities of both the faecal and feed materials, with reported values of 3.2–9.2 cm s^{-1} for Atlantic salmon faeces (Cromey et al., 2002a; Chen et al., 2003; Bannister et al., 2016) and 8.5–12.8 cm s^{-1} for uneaten feed (Chen et al., 1999; Riera et al., 2017), while a much weaker horizontal component is induced by the transfer of horizontal momentum from the surrounding currents. Modern fish farms are increasingly situated in more dispersive

* Corresponding author at: Institute of Marine Research, Postboks 1870 Nordnes, 5817 Bergen, Norway.
E-mail address: marcos.carvajalino.fernandez@hi.no (M.A. Carvajalino-Fernández).

https://doi.org/10.1016/j.marpolbul.2020.111685
Received 9 April 2020; Received in revised form 14 September 2020; Accepted 14 September 2020
Available online 08 October 2020

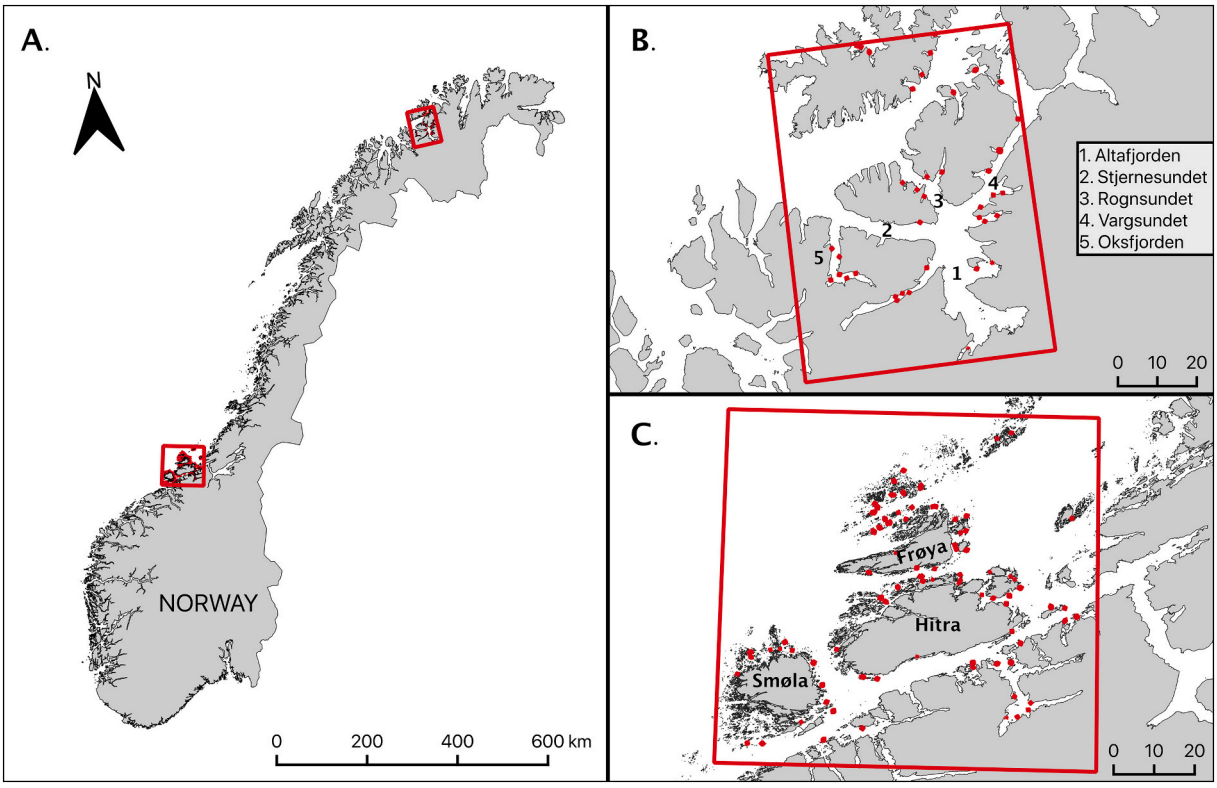

Fig. 1. Location of the two simulation domains along the Norwegian coastline (A). Altafjorden (B), in the northern county of Finnmark, hosts aquaculture sites in protected locations inside the fjord, while Frøya Archipelago (C), in mid-Norway, is representative for coastal exposed locations. Existing farms are shown as red markers. (For interpretation of the references to colour in this figure legend, the reader is referred to the web version of this article.)
Data source: Norwegian Directorate of Fisheries (accessed: 16.Dec.2019).

locations, where the horizontal transport can be substantial, impacting the extent of the POM footprint (Broch et al., 2017).

Once settled, POM does not remain static but is subject to a plethora of processes that can further mobilize the material along the seabed or across the water column, modify the structure of the particles or facilitate the assimilation of their constituents into the substrates or the trophic chains of the surrounding biological communities (Bannister et al., 2016; Law et al., 2016; Broch et al., 2017; Woodcock et al., 2018; Keeley et al., 2020). Among these processes, the resuspension of particles plays a noteworthy role in the extension of the POM footprint by redistributing the material from highly energetic areas towards more quiescent sites, sometimes kilometers away from the farms; as reported by the analysis of terrestrial fatty acids or isotopes within neighboring biological communities (Sarà et al., 2004; Woodcock et al., 2018; Woodcock et al., 2019). Particle resuspension is caused by the correlated fluctuations of the vertical and horizontal components of the turbulent velocity vector that occur in close proximity to the seabed, represented in terms of the bottom shear stress (τ_b). The bottom shear generates a set of lift and drag forces that detach the particles from the bottom and transports them into the overlaying current fields, should the bottom shear exceed a prescribed threshold called the critical shear stress (τ_c), which is strongly case-dependent (Henry and Minier, 2014; Law et al., 2016; Traugott and Liberzon, 2017). Therefore, accurate assessment of the critical shear for particle wastes from fish farms is fundamental to being able to predict the impact of fish farms upon the surrounding environment.

Several studies have examined the factors that influence POM resuspension in aquaculture and proposed parametrizations to include this process into numerical models, but the early approaches have proven to be overly simplistic. The seminal work by Cromey et al. (2002b) reported a τ_c value of 0.018 Pa to resuspend the POM from Atlantic salmon farms, but made no distinction with respect to waste type (i.e. faeces or feed). Subsequent studies revealed that a range of particle sizes existed, with presumably varying τ_c values, and that the 0.018 Pa threshold was more indicative of the lower end of the particle size spectrum for POM (Chamberlain and Stucchi, 2007; Weise et al., 2009). Early modelling efforts therefore gave larger erosion rates and material transport than was observed in the field (Chamberlain and Stucchi, 2007; Keeley et al., 2013; Chang et al., 2014). More recently, Law et al. (2016) and Carvajalino-Fernández et al. (2020) have established that substrate texture plays a major role on the resuspension of POM, and thus τ_c values should be defined using a substrate-dependent approach. Both studies identified differential critical thresholds for representative substrates in salmon fish farming locations, obtaining similar values for feed and faeces ranging from 0.04 to 0.06 for mud (smooth substrates), 0.08 to 0.12 for sand and 0.28 to 0.32 for cobblestones/fragmented rock.

In this study, we aim to close an important knowledge-gap by developing a substrate-dependent resuspension module, using the set of thresholds for faeces resuspension reported by Carvajalino-Fernández et al. (2020), and integrating them into a Lagrangian particle tracking model. We use this model to simulate particle spread in two farming locations along the Norwegian coastline, and compare the results against two control scenarios, one that includes no resuspension and one that uses the widespread, constant τ_c value reported by Cromey et al. (2002b). By comparing no-resuspension, constant-value and substrate-dependent resuspension scenarios, we evaluate whether the inclusion of the new substrate-dependent approach for particle resuspension provides a better prediction of the extent of the POM footprints beneath fish farms. This will give researchers involved with the modelling of aquaculture environmental impacts a clear direction on the way forward for further model development.

2. Materials and methods

2.1. Area of study and farming locations

Simulations were run for two locations with markedly different hydrodynamic regimes along the coast of Norway (Fig. 1A). The locations were chosen due to their high number of active, large-scale Atlantic salmon fish farms and the availability of extensive monitoring data suitable for model validation; the latter as part of two Norwegian Research Council (NFR) financed projects focused on studying the effects of salmon aquaculture upon benthic ecosystems. Under those projects, both areas were multibeam surveyed by the Norwegian Geological Survey (NGU) to provide high resolution bathymetry and substrate maps.

Altafjorden (70.2°N; 23.1°E, Fig. 1B) is an example of a sheltered, sub-arctic fjord system with an expanding aquaculture industry. The main body of the fjord is oriented towards the North-West, with a length of 30 km and a maximum width of 14 km (Wassmann et al., 1996). The fjord opens to the Barents Sea via three narrow inlets (Stjernesundet, Rognsundet and Vargsundet), from which several minor branches originate. Fjord depths range from 50 m at the sills in two of its sea-bound openings to over 450 m near the confluence of the three inlets and the main fjord. Altafjorden has a relatively strong semi-diurnal tidal excursion, with an amplitude between 1.5 and 2.5 m, that generates complex current patterns inside the fjord due to the interplay between the inlets' orientation with regards to the coast-following tidal wave, the Earth's rotational effect and the fjord's topography (Skarðhamar et al., 2018).

To date, there is a total of 33 licensed salmonid fish farms inside Altafjorden and its inlets, with a total licensed capacity of around 156,000 metric tons (Directorate of Fisheries, 2019). Two out of those farms, named Farm A1 and Farm A2 hereafter (Fig. 2), were selected for the simulations based on the amount of available data for model set-up and subsequent validation. Farm A1 is located on the Western coast of Oksfjorden (a secondary branch of Stjernesundet) while Farm A2 sits in a small embayment in Vargsundet, both locations have a bottom depth close to 130 m. The farms have a joint biomass capacity of 9000 metric tons, and are situated in sheltered areas of the fjord, which typically indicates rather calm hydrodynamic conditions and low velocities near the bottom.

Both farms in Altafjorden are located upon primarily rocky substrates, with the seabed at Farm A1 dominated by a mix of rock, gravel and sand, as well as pure bedrock with a slight unconsolidated layer of sediment. On the other hand, Farm A2 is situated over two similar sized sediment banks, one comprising sand with different amounts of incorporated gravel and one formed mostly by larger rocks, gravel and sand (Fig. 2).

The second location, *Frøya Archipelago* (63.6°N; 8.6°E, Fig. 1C), is representative of the highly dynamic, exposed coastal locations in Mid-Norway. The archipelago consists of the main islands Frøya, Hitra and Smøla, as well as a high number of small islets and skerries. The sea-bottom is rather shallow within the location, with the deepest areas (300–350 m) situated in the large banks to the East and West of Frøya island, while most of the channels between the main landmasses range from 30 to 100 m in depth. The archipelago is exposed to the open ocean conditions in the Norwegian Sea, with frequent influence from storms and waves generated offshore, however, the numerous islands dampen most of the swell.

Frøya Archipelago hosts a vast aquaculture industry, with farms located mostly around the coast of the main islands. The location rears close to 20% of the total Norwegian Salmonid production (Grefsrud et al., 2018), with a total biomass capacity of around 373,000 metric tons distributed among 94 licensed farms (Directorate of Fisheries, 2019). A total of six farms, clustered in pairs for the analysis due to their proximity, were selected for the simulations (Farms F1, F1 II; F2, F2 II; and F3, F3 II). These farms are situated over highly heterogeneous

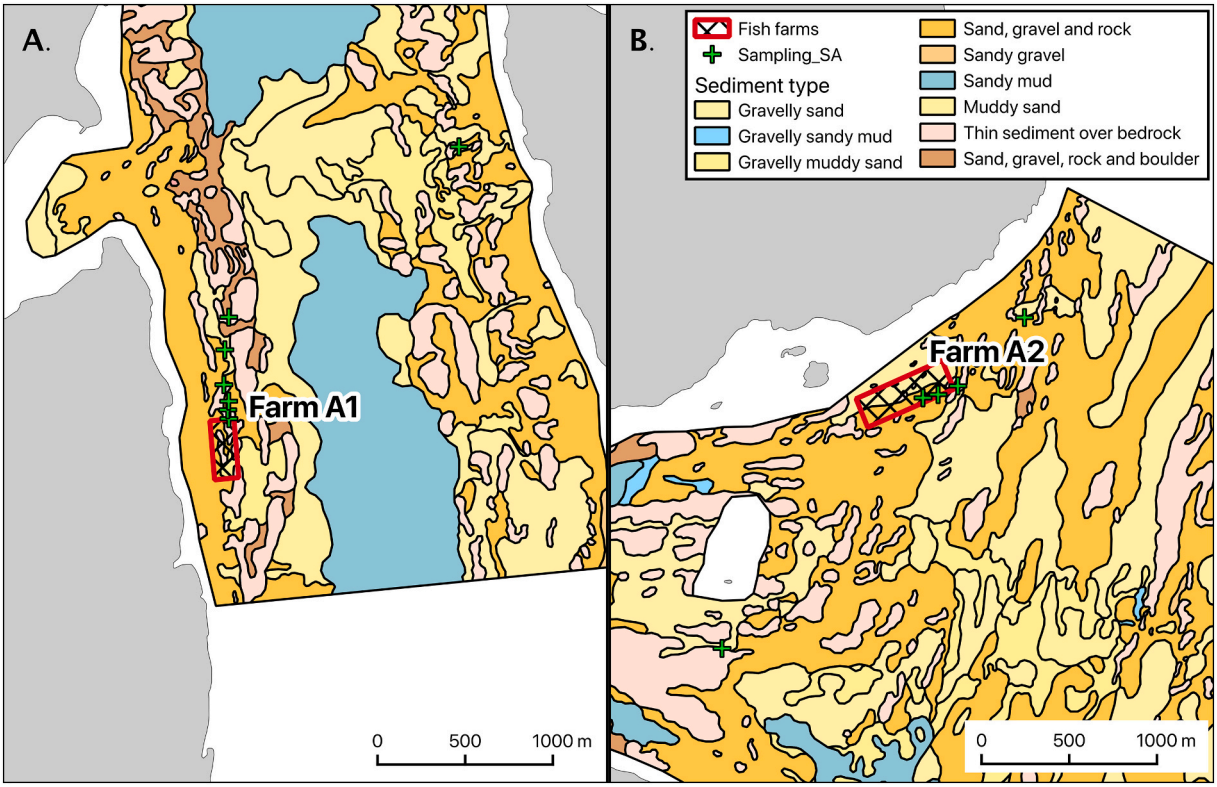

Fig. 2. Sediment characteristics at the selected farms in Altafjorden. Both locations are placed above rocky substrates, with sediments beneath Farm A2 (B) being slightly sandier and more unconsolidated than in Farm A1 (A).
Data source: Norwegian Geological Survey, Norwegian Directorate of Fisheries.

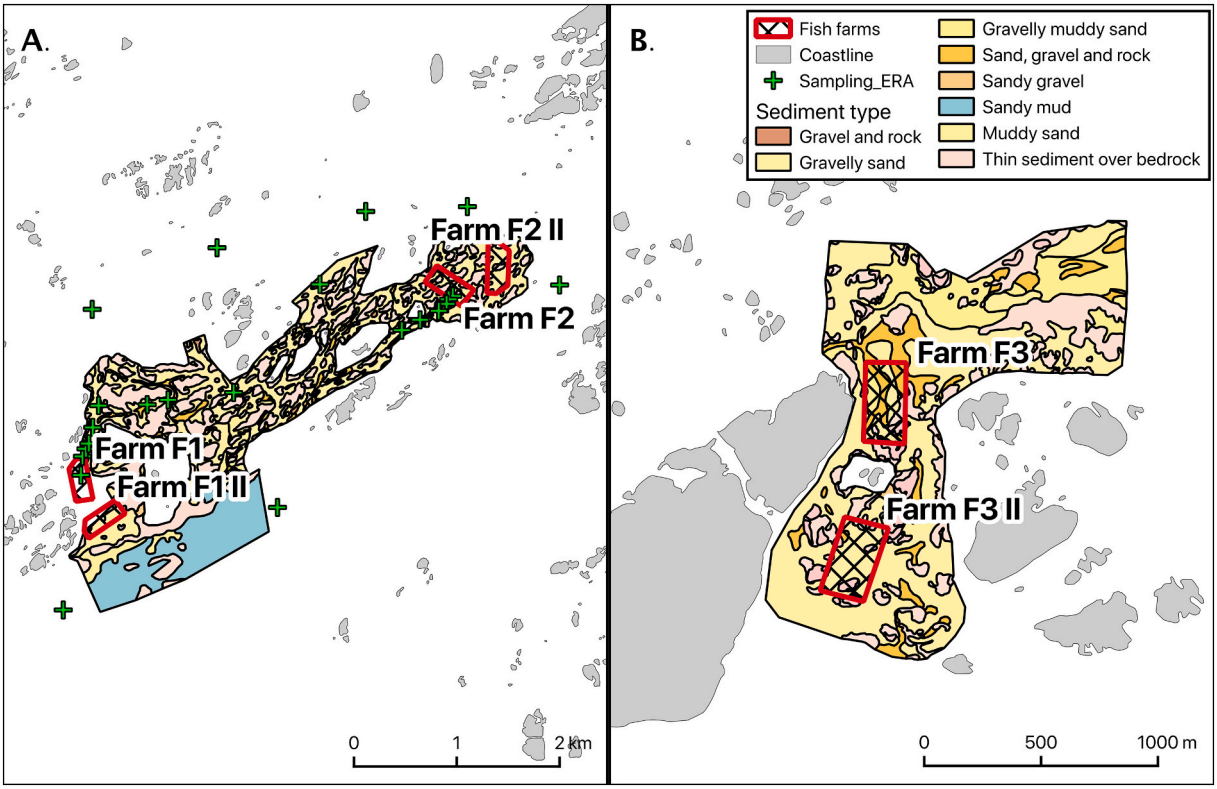

Fig. 3. Sediment characteristics beneath the selected farms in Frøya Archipelago. Farm clusters F1 and F2 are located in the north-western coast of Frøya Island, while the Farm F3 pair is located among a group of skerries in the northern part of the archipelago, bordering the open sea.
Data source: Norwegian Geological Survey, Norwegian Directorate of Fisheries.

and very shallow bottoms, constituted mostly by a mixture of medium to coarse sands with diverse amounts of gravel and shells and with depths between 30 and 40 m (Fig. 3).

2.2. Modelling system

Simulations were performed using an offline-coupled modelling scheme comprised of a hydrodynamic model and a Lagrangian particle tracking model. This modelling scheme was favored over online-coupled Eulerian alternatives due to the flexibility that a Lagrangian model provides in terms of serving individual particles with specific characteristics, as well as its potential for expansion for more complex processes with a relatively low computational cost and coding effort.

2.2.1. Hydrodynamic model

Dynamic ocean circulation fields of the full ocean state were simulated with the open-source Regional Ocean Modeling System (ROMS, see e.g. Shchepetkin and McWilliams, 2005, http://myroms.org; Haidvogel et al., 2008), which is a three-dimensional, free-surface, hydrostatic, primitive equation ocean model that uses generalized terrain-following S-coordinates in the vertical. ROMS comes with a variety of lateral boundary conditions, including open, closed, and periodic (Marchesiello et al., 2001). The Chapman (Chapman, 1985) and Flather (Flather, 1976) boundary conditions were used for the free-surface and the barotropic velocity, respectively. In our study, we provided radiation conditions on outflow and nudging to a known exterior value on inflow for 3D momentum and tracers, described thoroughly in Marchesiello et al. (2001), with a nudging on inflow 120 times larger than on the outflow. For vertical turbulence, the local closure scheme was based on the Generic Length Scale (GLS) parameterization (Umlauf and Burchard, 2003).

Two separate curvilinear, structured grids with a 160 m × 160 m resolution in the horizontal and 35 terrain-following vertical levels were used in the present work. The grids expanded over larger regions than the direct areas of influence of the objective farms, approximately adjusting to the limits of the Norwegian aquaculture production zones 6 (Nordmøre og Sør-Trøndelag) and 12 (West-Finnmark), as defined by the Norwegian Ministry of Trade, Industry and Fisheries (Nærings- og fiskeridepartementet, 2017), which include Frøya Archipelago and Altafjorden, respectively. Both grids were forced along the open boundaries with hourly inputs from a larger-scale coastal model, NorKyst800 (Albretsen et al., 2011) which covers the entire Norwegian coast. The NorKyst800 model was run using an 800 m × 800 m grid resolution in the horizontal and also applied 35 vertical levels. However, as the Frøya and Alta models were simulated for different years, 2015/2016 and 2018 respectively, different external forcing was applied to each of them. Daily river flow rates were computed by the HBV model provided by the Norwegian Water Resources and Energy Directorate (Beldring et al., 2003).

Lateral boundary conditions and initial field conditions for the NorKyst800 model for the 2015 and 2016 runs were retrieved from a Nordic Seas 4 km ocean model (Lien et al., 2014), which covers the area from the North Atlantic west of Ireland, to the Nordic Seas and into the Arctic to the north. The corresponding open boundary conditions for NorKyst800 for the 2018 runs were retrieved from the Norwegian Meteorological Institute's operational 4 km ocean model covering the same area of the Nordic Seas (data available at http://thredds.met.no). Tidal forcing from TPXO 7.2 (Egbert and Erofeeva, 2002) was imposed along the open boundaries of NorKyst800.

High-resolution atmospheric forcing was used in NorKyst800 and the 160 m-models. The 2015 and 2016 simulations used inputs from a 3 km × 3 km version of the Weather Research and Forecasting model (WRF, see http://www.wrf-model.org and Skamarock et al., 2008) developed by the National Center of Atmospheric Research (NCAR). For the 2018 run, the atmospheric forcing was obtained from the 2.5 km × 2.5 km AROME MetCoOp forecasting system at the

Norwegian Meteorological Institute (Müller et al., 2017).

Bottom shear stress was calculated using a quadratic drag extrapolation from the velocity at the bottom-most computational layer in the model (Warner et al., 2008) using a constant quadratic drag coefficient of 0.003.

2.2.2. Lagrangian particle tracking model

The distribution and transport of faeces from the selected open cage salmon aquaculture locations was calculated using an open access Lagrangian model (LADIM, Ådlandsvik and Sundby, 1994, https://github.com/bjornaa/ladim). The model is coded in Python and based upon a Lagrangian version of the advection-diffusion equation, where advection terms are obtained from the velocity fields calculated by the hydrodynamic model—via offline coupling—while the diffusive part (sub-grid turbulent motions) is calculated using a random-walk term. The general transport equation is given by

$$\Delta x_i = U_i \Delta t + R \sqrt{2 \Delta t K_i}$$

where Δx_i is the change in particle position along the axis i, U_i is the particle's advective velocity, Δt is the timestep, R is a random number taken from the standard normal distribution and K_i is the dispersion coefficient. In this study, the particle's advection velocity in the horizontal was calculated using a 2nd order Runge-Kutta scheme with a timestep of 30 s, while a Euler forward stepping scheme was used for the vertical velocities. The horizontal dispersion coefficient (K_i) was set to 1 $m^2\ s^{-1}$.

Additional particle-specific processes, such as vertical dispersion, resuspension, consumption or degradation can be integrated into the LADIM code using an individual-based modelling (IBM) approach. For the present study, a new resuspension IBM module was developed, which is available in an online git-repository (https://github.com/pnsaevik/ladim_plugins, version 1.2.1) for further community-development. In the module, settled particles in which the bottom shear stress exceeds the critical shear value are flagged as "resuspended" and re-entrained into overlaying flow using a random walk scheme for space-varying diffusivity (Visser, 1997; Nordam et al., 2019). Diffusivity increases linearly from the bottom according to the "law of the wall" (Lynch et al., 2015) up to a maximum value of 0.01 $m^2\ s^{-1}$. Time step length equals the advective time step. Particles that hit the bottom after being resuspended are reabsorbed into the seabed.

Potential sources of uncertainty in the Lagrangian model, such as the value for the horizontal and vertical dispersion coefficients, release depth and simulation timestep were evaluated during the model development phase. The aforementioned values for the parameters were selected based on existing bibliography (e.g. Martin and McCutcheon, 1999; Okubo and Levin, 2001), empirical knowledge and best fit in comparison to the field observations.

2.3. Emission characteristics and particle-specific processes

Simulations were performed for different periods in the two locations, covering different stages of a typical 18 month production cycle for Atlantic Salmon and trying to match the sampling campaigns from the coinciding NFR projects in the area (Table 1). Farms in Frøya Archipelago started an almost simultaneous production cycle between February and March 2015, allowing a complete follow-up of the waste emission levels at different growth stages during this study. The two farms in Altafjorden put the fish into the cages at different times, around Oct–Dec 2016 for Farm A1 and in May 2017 for Farm A2, and monitoring data were only available for their respective peak periods. In addition to some farms starting production at differing times, two farms (one in each region) had to harvest out the fish earlier than scheduled due to disease outbreak. Therefore, the stage of the overall production (i.e. early, mid, peak) should only be used as a rough indicator of the total biomass present in the pens at a given simulation period.

Table 1
Simulation times and production data for the selected.

Stage	Simulation dates	Number of farms	Total biomass [t]
Frøya Archipelago			
Early production	15.07.2015–01.09.2015	6	2575–6700
Mid production	15.01.2016–01.03.2016	6	15,070–19,655
Peak production	15.04.2016–01.06.2016	4–6	17,060–13,340
Altafjorden			
Peak production A1	15.05.2018–01.07.2018	2	5115–3850
Peak production A2	15.10.2018–01.12.2018	1	3850–1070

Monthly feed use during the simulation periods was obtained directly from the farmers and used as a proxy to estimate the amount of faeces emitted by each farm. A feed-to-faeces conversion factor of 20% was used following Cubillo et al. (2016) and the number of particles released into the model was defined such that each particle represented 1 kg of faeces. We used the concept of "super-individuals" in accordance to Scheffer et al. (1995) to represent one thousand elements within a single particle, allowing us to simulate POM to the gram level. The particles were released from the cage bottom (fixed at 20 m) at an hourly basis, distributing the particles randomly inside the licensed farm polygons obtained from the Norwegian Directorate of Fisheries (Directorate of Fisheries, 2019).

The particles were initialized with sinking velocities in accordance with the distribution reported in Bannister et al. (2016), where faecal particles were tested on a settling column and vertical velocity was mapped to 7 velocity classes (Table 2). In Bannister et al. (2016), settling velocities were observed for three different fish size classes; however, we assumed the effect of the inter-class differences to be minimal when compared to other potential sources of variability, and thus neglected in our study. Particles were randomly allocated a settling velocity from the distribution based on a within-interval uniform randomness assumption.

As the current version of the model does not include a benthic response module, a maximum lifespan had to be imposed to the particles to allow an accurate depiction of the POM footprints. Given the paucity of information in the literature regarding the structural stability of faecal pellets, a conservative value of 12 days was selected as particle lifespan. After this point, the particles were assumed to be consumed by biological organisms or physically degraded to a point they could not be further simulated as intact faecal pellets.

Simulation results were reconverted from faeces to total POM values using a scaling factor of 1.25. This assumes that faeces correspond to approximately 80% of the particles emitted in a farm, following Cubillo et al. (2016), whereas the rest of the material corresponds to uneaten feed.

2.4. Particle transport scenarios

Three scenarios for particle transport were simulated for each emission period: a first control scenario with no resuspension (S1) and

Table 2
Settling velocity distribution for salmon faecal material.
Source: Bannister et al. (2016).

Proportion of particles [%]	Settling velocity [cm s^{-1}]
66.2	5.0–10
18.9	2.5–5.0
3.2	1.5–2.5
2.6	1.0–1.5
2.8	0.5–1.0
6.3	< 0.5

two scenarios that include resuspension, one (S2) using a constant critical shear stress value of 0.018 Pa, following Cromey et al. (2002b), and the other (S3) using the set of substrate-dependent resuspension thresholds from Carvajalino-Fernández et al. (2020).

While there is no further transport after the initial settling of the particles to the bottom in S1, scenarios S2 and S3 query the model at each time step for settled particles. The bottom shear stress for these particles is calculated from the velocities in the hydrodynamic model and compared against the given critical shear value for resuspension. In S2, the constant 0.018 Pa threshold was set in the Lagrangian model's IBM module, while the S3 scenario retrieves the substrate type at the particles' location from high-resolution bottom survey shapefiles around the farm, which are publicly available at the Norwegian Geological Survey website (http://geo.ngu.no/kart/marin_mobil/). Substrate types are then assigned the critical shear values corresponding to the 4 standard sediments reported in Carvajalino-Fernández et al. (2020).

2.5. Results correction for sediment trap comparison

Model results were compared against POM depositional flux measured using sediment traps consisting of 4″ PVC tubes attached to custom-fit metallic frames on a mooring line, located approximately 2 m above the seabed. The traps were positioned every 50–200 m along 600 m to 2 km long transects extending from the closest point to the farm's center that the mooring lines allowed and were recovered after 7 to 8 days. Two traps were used per deployment and duplicate subsampling was taken from each trap during each of the simulated periods for Farms A1, A2, F1 and F2 and analyzed as described in Keeley et al. (2019).

Sediment traps cover only a fraction of the area that is influenced by the particles, and thus associated sampling errors must be taken into account and corrected when comparing the observed and simulated values. A linear regression model, similar to the one used in Cromey et al. (2012) for feed pellets, was implemented based on the following equation:

$$POM_{obs} = \beta_1 (POM_{mod}) + B \quad (1)$$

where POM_{obs} and POM_{mod} are the observed and modeled depositional fluxes, respectively, β_1 is a scaling factor, intended to account for the discrepancies between model and observations due the sampling errors inherent to the sediment traps, and B is the local background POM flux.

3. Results

3.1. Hydrodynamic conditions

Sites in Altafjorden showed similar trends in their velocity profiles, with the highest values and a strong gradient in the upper 10–20 m of the water column followed by a more stable deep layer (Fig. 4). This pattern is consistent with typical fjord circulations, where riverine input, together with wind-induced momentum and entrainment, generates a thin layer of fast-moving water above a slower, intermediate layer, where transports are determined by pressure (density) gradients along the fjord axis. The depth-averaged velocity (DAV) for the two locations was fairly similar, with values of 5–10 cm s^{-1} below 20 m depth. While larger variability can be seen in Farm A2, both sites show important fluctuations in their maximum values at different depths, a potential indicator of transient density currents.

Farm sites in Frøya Archipelago showed less variability in their simulated velocity profiles than their counterparts in Altafjorden (Fig. 4), which can be attributed to the lack of a stabilizing fresh water layer, as well as a relatively shallow depth, promoting well-mixed conditions in the vertical and potentially larger excursions of the surface and bottom boundary layers. In terms of DAV, Farm F1 showed the lowest average velocities with ca. 5 cm s^{-1}, while F3 and F2 registered 10 and 15 cm s^{-1} respectively, the latter showing significantly larger maxima and standard deviations. Disregarding the difference in DAV, all sites showed near-bottom velocity maxima of 3–5 times their mean value, indicating a high potential for resuspension episodes considering the type of substrate beneath the farms.

Daily-averaged bottom shear stresses were relatively similar for both farms in Altafjorden during the first simulation period (Peak A1), with a median close to 0.06 Pa but slightly larger variability at Farm A1 (Oksfjorden). During the second simulation period (Peak A2), more dynamical conditions seem to be present in the area, with noticeable differences between the sites and even larger shears calculated for Farm A1, with median value around 0.1 Pa (Fig. 5). Maximum shear stresses calculated in the direct area of influence of the farms were close to 0.3 Pa.

The calculated mean bottom shear stress among the farms in Frøya Archipelago maintained a very stable pattern between the simulations. Farm F1 registered the weakest shear among the sites, with values usually ranging from 0.03 to 0.08 Pa, and occasional daily means between 0.1 and 0.3 Pa. Farms F2 and F3 had similar median values around 0.1–0.15 Pa, with much higher variability being registered at Farm F2. The Mid production period (January 2016) was the most dynamic simulation, due mainly to the higher frequency of storms in the Norwegian Sea during winter.

The bottom shear values reflect the positioning of the farms. F1 is located behind a series of islets and skerries in the SW – NE direction, which shelters it from the direct effect of the coastal trapped, tidal Kelvin wave that follows the Norwegian coastline. Even if Farm F2 has the same orientation as Farm F1, it is much less sheltered and therefore receives a more direct influence of the tide and the wind. Farm F3 is located at a small inlet, oriented SE – NW, which reduces the effect of the coast following tidal waves but further exposes it to the swells generated by the storms in the Norwegian Sea.

3.2. Particulate material transport and dispersion

The extent of POM influence upon the seabed during a given production stage was determined using 80 m bin-averaged accumulation maps, taking special care not to count the same particles multiple times once they were settled (Figs. 6 and 7). Contour maps were generated using 1 g m^{-2} d^{-1} as the lower limit of POM deposition where hypoxic or anoxic conditions, and thus negative impacts, start forming in sediments under finfish aquaculture sites, according to Hargrave (2010) and references therein. Even if the model is based on a coastline with the same resolution as the hydrodynamic model, a detailed coastline is used in the plots for illustration purposes.

The farms in Altafjorden showed a well-defined elliptical deposition footprint, with the largest accretion of organic material close to the farm's centroid and the depositional fluxes monotonically decreasing away from it, generating near-concentric contours around the farms (Fig. 6). A deviation from this pattern was observed for the S2 scenario, particularly in Farm A2, where the enhanced material spread due to resuspension with a low critical shear shifted the footprint's center of mass to a position southwest to the farm. Smaller deposition centers, with flux values of 1–4 g m^{-2} d^{-1} of POM, were also observed following the coast towards the northeast, in areas that were not affected in the other scenarios. The maximum values for depositional flux in Altafjorden were close to 42 g m^{-2} d^{-1} for both farms, during respective peak periods. At the same time, the total affected area for Altafjorden—when using 1 g m^{-2} d^{-1} as the threshold for POM impact—ranged between 63 and 125 Ha for all periods, with as much as 50–95% of this area corresponding to fluxes below 5 g m^{-2} d^{-1} (Table 3).

When resuspension was added to the simulations in Altafjorden, the material originally settled during the control case (S1) was redistributed in different ways according to the approach (scenario) being used. For both production periods, S2 caused a transport of POM from

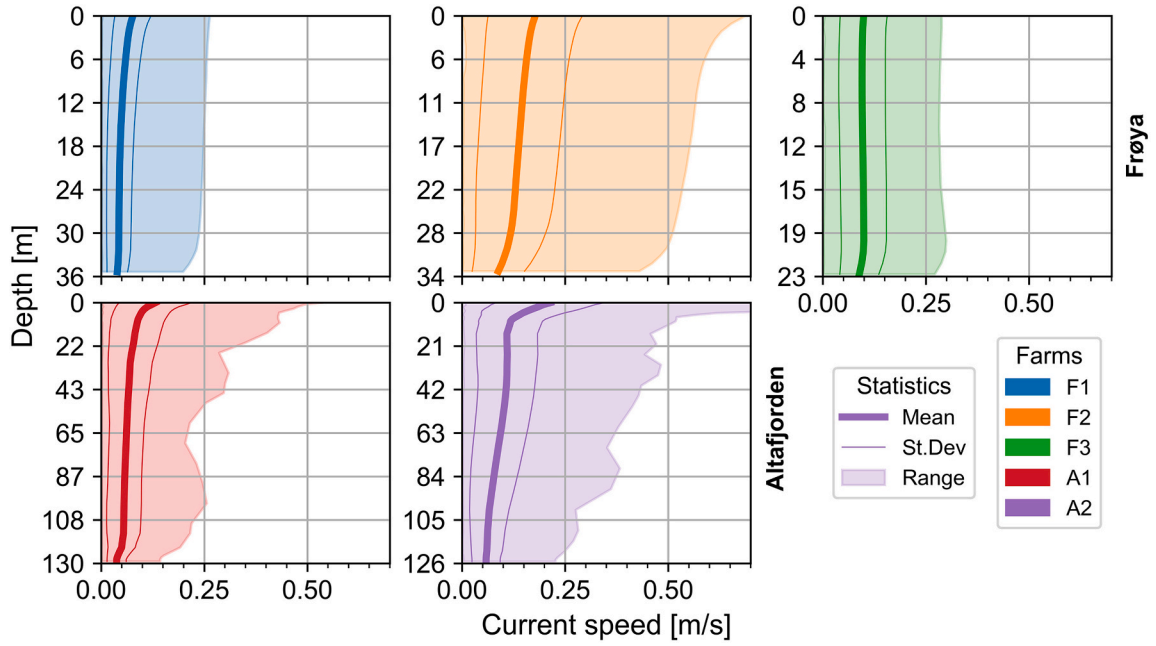

Fig. 4. Vertical profiles of modeled current speed at the selected farms. The profiles correspond to the mid production period for Frøya Archipelago (upper panel, winter season) and period Peak A1 for Altafjorden (lower panel, both farms in operation).

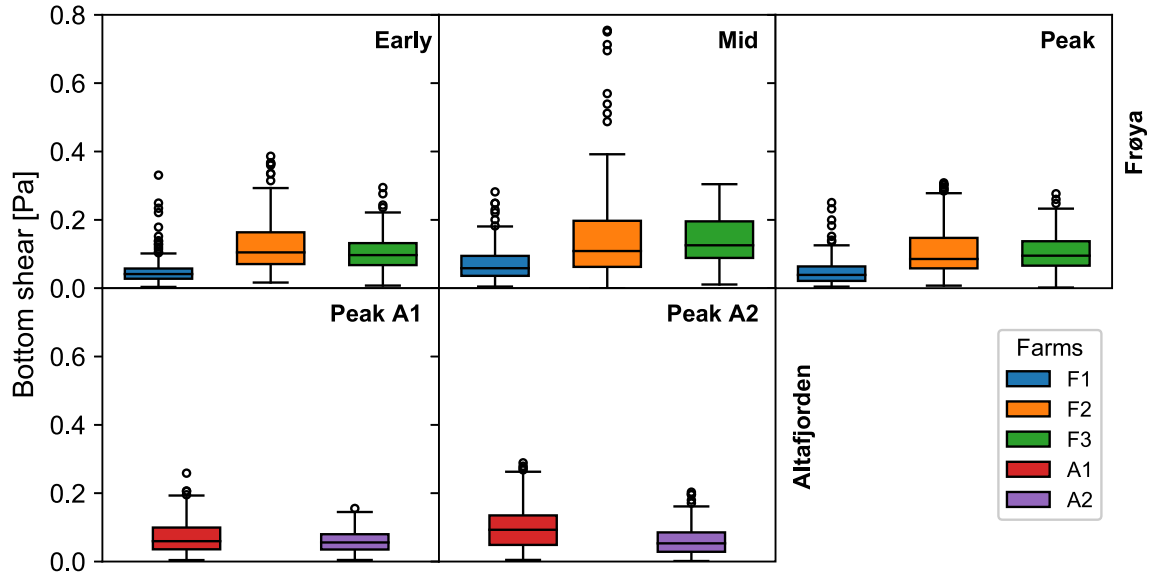

Fig. 5. Daily averaged bottom shear stresses calculated by the hydrodynamic model for Frøya Archipelago (Upper panel) and Altafjorden (lower panel). Values are calculated as the mean of the cell directly at the farm centroid and the 9 contiguous cells in the model grid.

areas originally exposed to high fluxes towards the outer regions of the footprint, driven solely by the strength of the bottom shear and the amount of material available for resuspension. This transport pattern causes a strong reduction in the extent of intensely influenced area near the farm centroid and increases the total extension of the footprint around its peripheries, moving the POM towards previously unaffected locations. On the other hand, the influence of substrate type in S3 imposes an extra spatial constrain to the potential for particle resuspension, concentrating the material towards the center of the farms and therefore attaining overall farm footprints slightly smaller than the non-dispersive case. This can be a consequence of the large banks of rocky substrate located beneath the farms, which require a bottom shear stresses in the order of 0.3 Pa to remobilize the particles in the S3 scenario, a condition that seldom occurs in the location (Section 3.1). Material that has been transported from the sandbanks into the rocky substrates will effectively be trapped there for the rest of the simulation, a phenomenon that was observed during video surveys in the area.

Unlike the farms in Altafjorden, POM footprints at Frøya Archipelago deviated strongly from the characteristic elliptical shape observed in most non-dispersive sites. Footprint results from the baseline scenario (S1) agree quite well with those recently reported in Broch et al. (2020) for the same farms. POM footprints at both farm clusters F2 and F3 followed the direction of the main tidal flow, with expansion of their area of influence towards the North and Northeast. On the other hand, the farm cluster F1 showed a more localized accumulation of material near the westernmost corner of the footprint, with an expansion of the area of influence towards the south with the use of the low critical-shear S2 scenario (Fig. 7).

Simulations during the mid-production stage in Frøya, where the largest emissions were effectively generated, reported maximum values

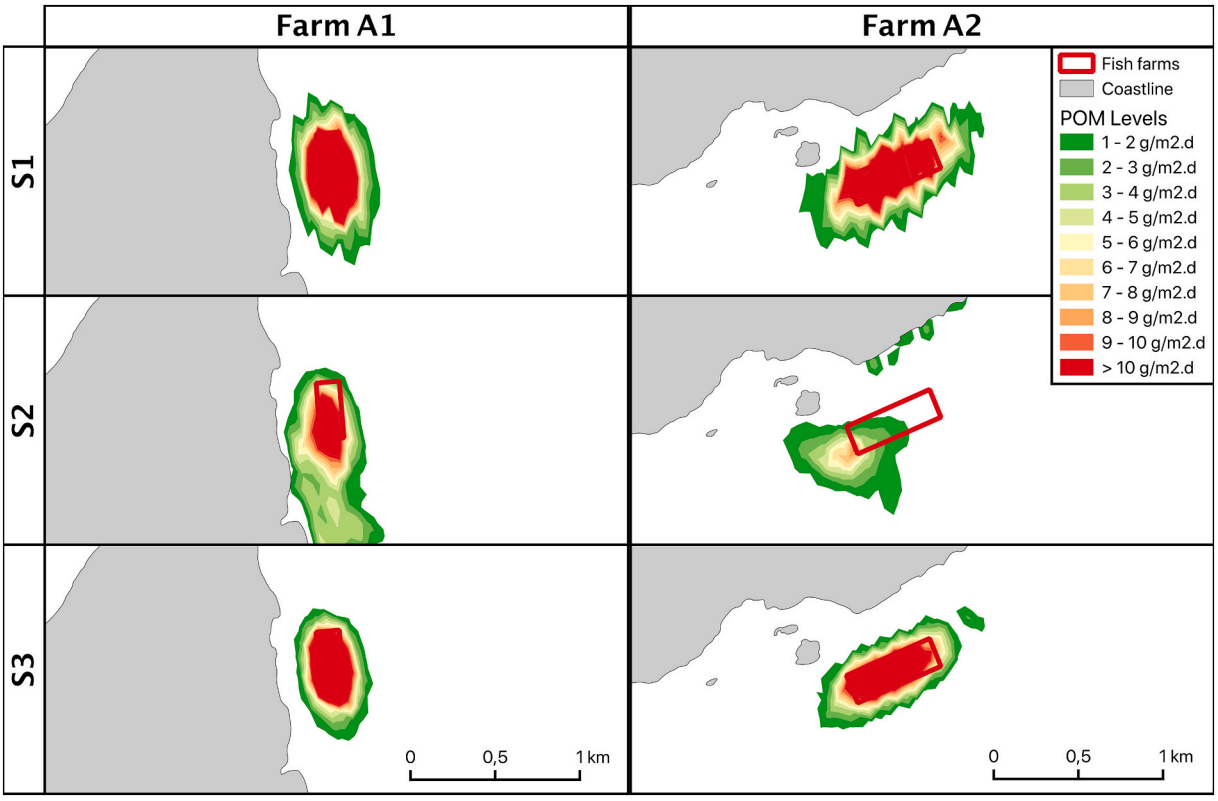

Fig. 6. Average depositional POM footprint for Peak period A1 using "no resuspension" (S1 – upper panels), "constant threshold" (S2 – mid panels) and "substrate-dependent" (S3 – lower panels) scenarios in Altafjorden.

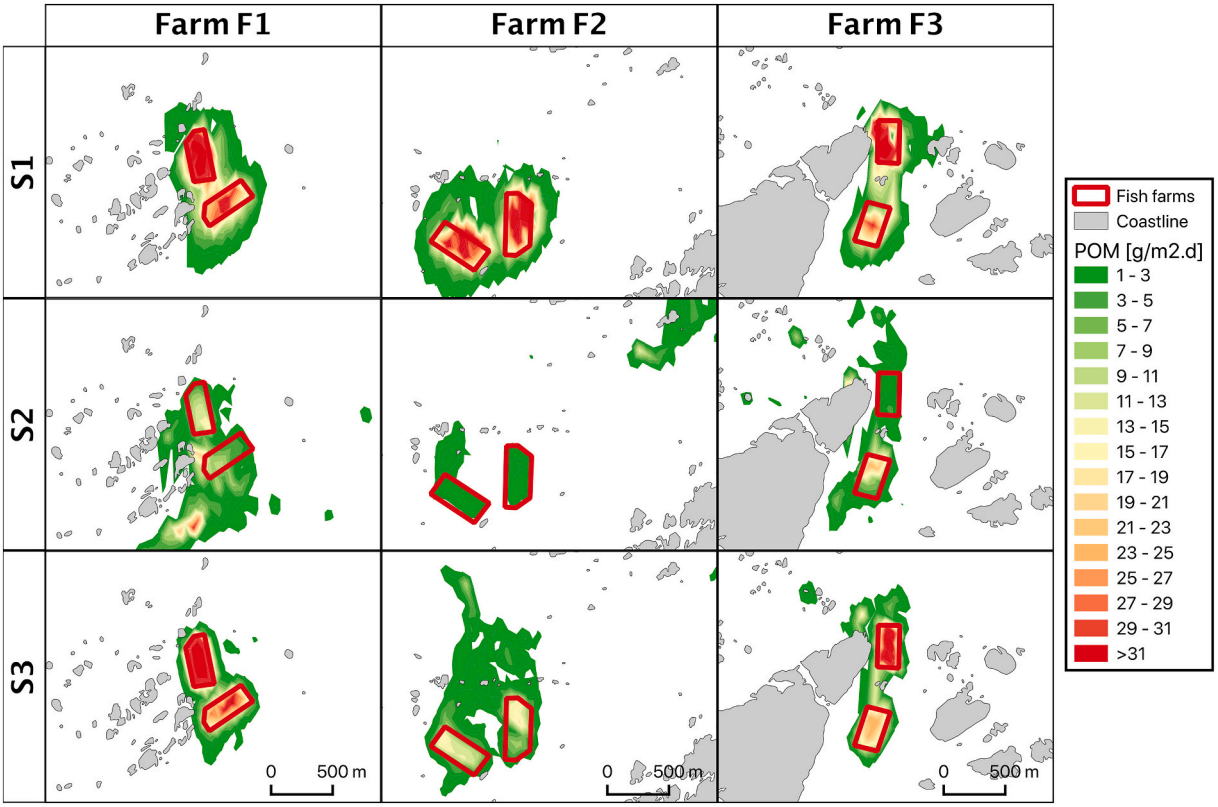

Fig. 7. Average depositional POM footprint during mid production in Frøya Archipelago when using a "no resuspension" (S1 – upper panels), "constant threshold" (S2 – mid panels) and "substrate-dependent" (S3 – lower panels) resuspension scenarios.

Table 3
Areal extent of the POM footprint for different mean depositional fluxes [g m^{-2} d^{-1}] in Altafjorden. The shading represents the magnitude of the increase (red) or decrease (blue) of influenced area for resuspension-including scenarios when compared to the base case simulation (S1) during each stage.

Stage	Scenario	Area of POM influence [Ha]								
		Deposition flux [g m^{-2} d^{-1}]								*Total*
		1–3	*3–5*	*5–7*	*7–9*	*9–11*	*11–13*	*13–15*	*>15*	
Peak production A1	S1	34,2	13,42	8,52	6,85	5,24	5,03	4,41	14,1	91,77
	S2	64,14	20	5,98	3,59	1,96	1,38	1,1	1,84	99,99
	S3	22,1	9,16	6,1	4,6	3,96	3,5	3,06	10,51	62,99
Peak Production A2	S1	27,63	7,95	5,42	3,83	3,03	2,69	2,56	19,45	72,56
	S2	114,39	10,44	0,56	0	0	0	0	0	125,39
	S3	15,07	5,71	3,77	2,98	2,54	2,23	2,27	13,19	47,76

Table 4
Areal extent of the POM footprint for different mean depositional fluxes [g m^{-2} d^{-1}] in Frøya Archipelago. The shading represents the magnitude of the increase (red) or decrease (blue) of influenced area for resuspension-including scenarios when compared to the base case simulation (S1) during each stage.

Stage	Scenario	Area of POM influence [Ha]										
		Deposition flux [g m^{-2} d^{-1}]										*Total*
		1–5	*5–10*	*10–15*	*15–20*	*20–25*	*25–30*	*30–35*	*35–40*	*40–45*	*>45*	
Early production	S1	95,52	42,26	22,95	17,98	11,12	3,98	2,5	1,28	0,21	–	197,8
	S2	183,25	27,9	12,02	3,95	0,04	0	0	0	0	–	227,16
	S3	102,67	30,23	17,16	7,26	3,2	2,82	2,92	2,12	0	–	168,38
Mid production	S1	111,17	36,3	25,54	17,98	13,7	11,57	8,56	6	2,71	4,06	237,59
	S2	211,19	33,06	11,5	4,84	2,3	0,51	0,08	0	0	0	263,48
	S3	158,47	31,08	19,01	9,63	6,78	4,8	3,32	2,53	1,25	2,71	239,58
Peak production	S1	99,61	38,68	27,14	16,68	12,06	9,6	7,03	3,27	1,13	1,19	216,39
	S2	210,26	42,32	11,57	3,49	1,29	1,22	0,15	0	0	0	270,3
	S3	84,55	30,14	19,9	11,58	9,28	7,72	3,51	1,88	1,31	0,29	170,16

of 52.3, 42.7 and 62.4 g m^2 d^{-1} for farm clusters F1, F2 and F3, respectively. The total area influenced by POM during the simulations was in the order of 200–270 Ha, with the largest footprints in the resuspension scenarios during the mid and peak production stages (Table 4).

The general trend of material transport using S2 in Frøya was very similar to the one in Altafjorden, with a contribution of material from the higher flux areas towards the low flux fringes of the footprint, generating an overall flattening of the POM's spatial gradient outwards from the farm when compared to the control case S1. In contrast, S3 causes a more local pattern of material exchange, with transport occurring between neighboring footprint contours, given that the sediment type favors particle mobility, rather than the large-scale material relocation observed in S2.

3.2.1. *Validation against field observations*

Depositional fluxes were bin-averaged to a 40 m resolution grid in order to compare them with the field observations from the sediment traps. The use of a 40 m bin-averaging allows us to capture the differences between the sampling stations in the vicinity farm, which are

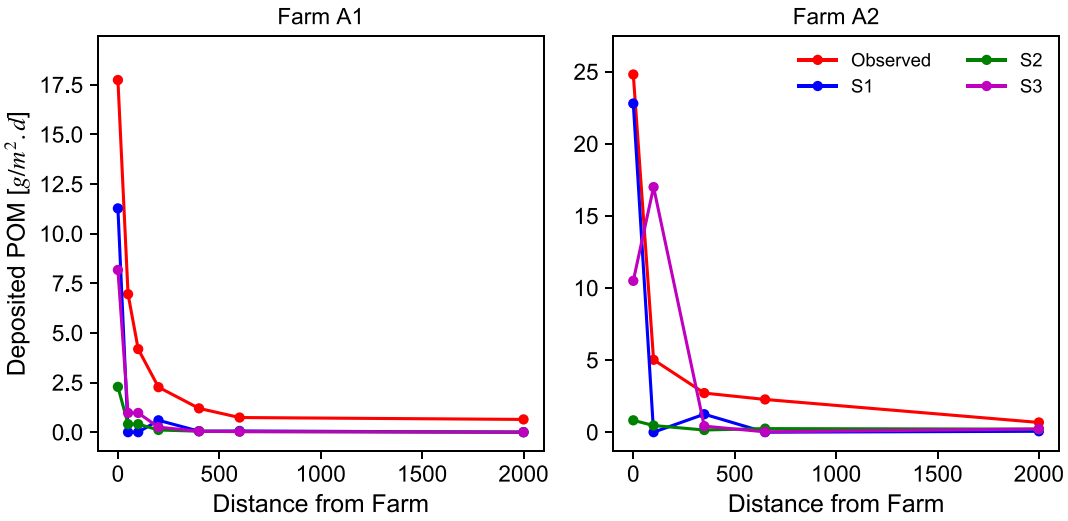

Fig. 8. Transect comparison for modeled values and field observations in Altafjorden. Results from Farm A1 (left) correspond to the Peak A1 period, while those from Farm A2 (right) were taken from the Peak A2 period. *The observed values are presented as mean* (*solid red line*) ± *the standard error of replicate sediment traps in the rig* (*hatching*). (For interpretation of the references to colour in this figure legend, the reader is referred to the web version of this article.)

separated by 50 m, but introduces a source of inaccuracy that has to be considered when analyzing the model's fit to the observations.

Model results in Altafjorden show a high deposition of POM over the first 500 m from the farms limits, leveling off to a constant flux over the rest of the transect (Fig. 8); a pattern that goes in line with the conventional enrichment gradients observed in the direct vicinity of the farms at non-dispersive locations. For Farm A1, scenarios S1 and S3 reproduce the gradient and shape of the observed fluxes satisfactorily, while for Farm A2 only S1 resembles the observed transect measurements. Both scenarios tend to underestimate the fluxes of material near the farm and show a constant gap between observed and modeled values at the leveling-off phase. The former can respond to inaccuracies in the emission parameters, such as intra-month variability in the feed input or feed-to-faeces conversion ratios, while the latter can be attributed to the magnitude of the background natural POM flux, which is not originally included in the model. For both farms in Altafjorden, S2 performed the worst when compared against the other two scenarios, with a very larger underestimation of the particle fluxes nearby the farms.

Simulations from Farm F1 in Frøya Archipelago (Fig. 9, left) show a high deposition of POM in the first 100 m of the transect for all scenarios, with a leveling off farther from the farm. This pattern is similar to the one in Altafjorden, but with a shorter spreading distance in consonance to the much shallower depths in the Archipelago.

The strong localized accumulation nearby the farm showed by the model can also be observed in the sediment trap records during mid-production, but lacks during the early production stage, where there is a smoother gradient in the close vicinity of the farms. The absence of data for the under-200 m segment at F1 during the peak period prevents verification of the predicted gradient for that scenario. However, if we assume that the tendency in the rest of the transect also applies to the missing region, we could expect a smoother reduction in the first 200 m of the observed transect than the one reported by the model. After 200 m, observations showed a leveling off of the deposition gradient for all simulation periods. This leveling off was also present in the model results, although with lower floor values than the observations. As with Altafjorden, this lower floor can be explained by the absence of the background POM fluxes in the model in some of the transects.

The pattern of POM deposition at Farm F2 was similar to Farm F1 (Fig. 9, right). However, the initial strong depositional gradient near the farm is less smooth and extends to 200 m from the farm, due to the larger exposition and the stronger currents in the location when compared to Farm F1. Modeled POM depositional flux in the immediate vicinity of Farm F2, i.e. the first 100 m, was closer to the observed values than in the case of Farm F1, especially during the peak production period.

As for the case of Altafjorden, scenarios S1 and S3 manage to resemble the observed patterns, with S3 widely outperforming the no-resuspension case for Farm F2. On the other hand, even if S2 managed to capture the initial steep gradient of deposition in Farm F1, it delivered an almost flat signal in Farm F2. This seems to indicate that the low value of critical shear stress in S2 performs poorly in highly dynamic environments such as F2, where the extra constraint of the sedimnent-dependent scenario yields the best results.

Results for the model correction procedure using Eq. (1). reflect the strong underestimation of the observed depositional fluxes in the close vicinity of the farm in Altafjorden, with observed values more than twice the model results (Table 5). Background deposition fluxes for the area rounded 2 g m^{-2} d^{-1}, which we consider in line with the quiescent nature of the fjord.

In the case of Frøya Archipelago, the correction procedure identified a high variability in the background POM fluxes, with values ranging from 0.5 to 8.0 g m^2 d^{-1}, which agree fairly well with the POM measured in remote reference stations (2.7–5.9 g m^2 d^{-1}) during the same surveys, as reported by Keeley et al. (2020). The scaling factors indicate a much lower error in this location than for Altafjorden, with period average R^2 values ranging from 0.4 to 0.8 (Fig. 10). We consider the low fit of results for the early production period in Farm F2 an outlier due to the unusual results in the sediment trap measurements for this period. In most cases the model still shows deviations of in the order of 20 to 60% of the values registered by the sediment traps.

The corrected transect profiles using the parameters indicated in Table 5 are included as Supplement I and Supplement II of the present manuscript.

4. Discussion

We identified significant differences in terms of footprint extent and material redistribution patterns between scenarios S2 and S3 for all studied locations, with S2 favoring larger spread of the footprint and even excursion of the material towards detached locations kilometers away from the farm. On the other hand, S3 displayed a more moderate trend of particle spread in relatively quiescent locations, with evidence of particle resuspension inside and in the close vicinity of the original footprint in the baseline scenario, at the same time as important particle remobilization in highly dynamic environments. Given the repeated

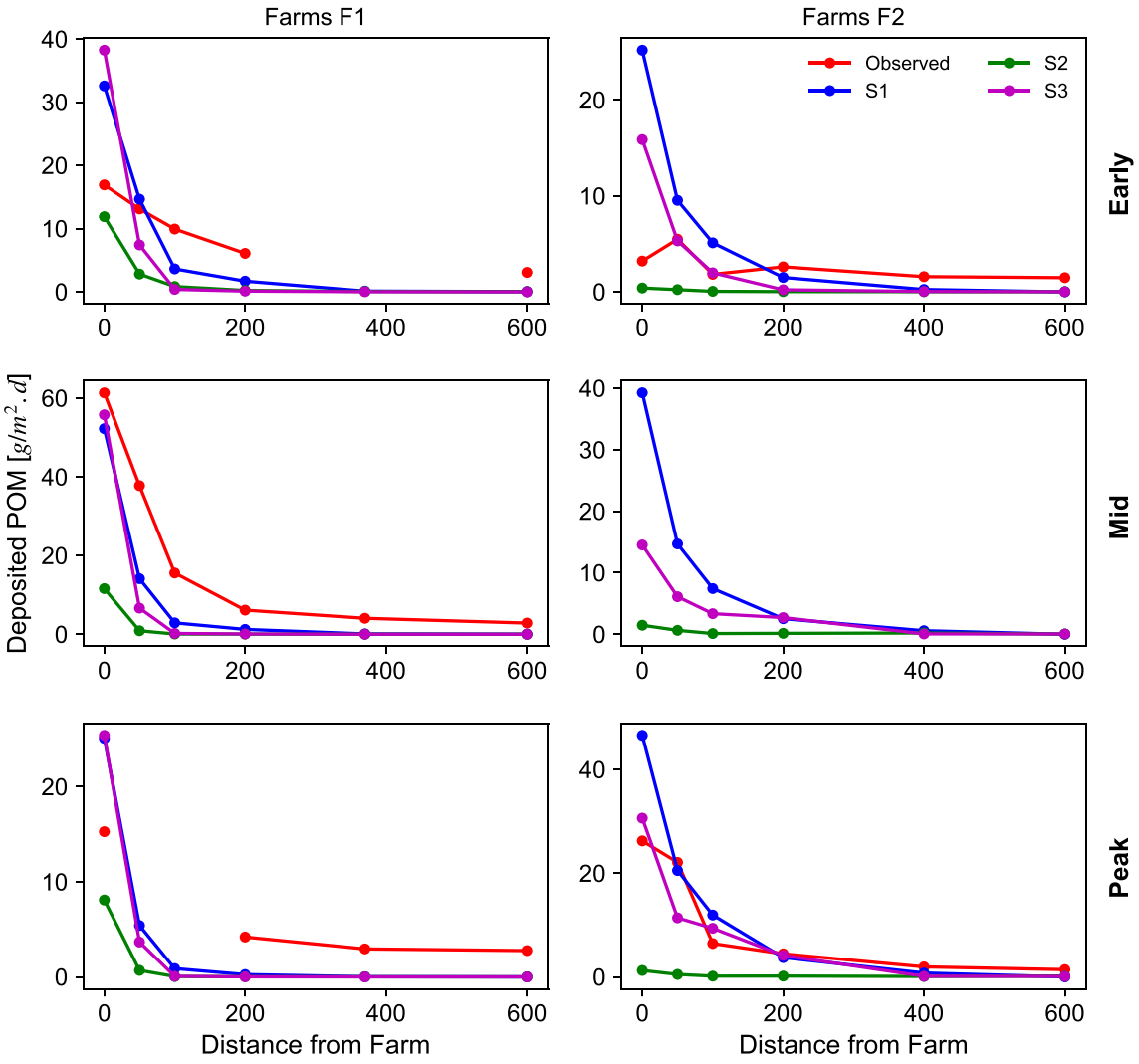

Fig. 9. Modeled vs. Observed POM values along the sampling transects in Frøya Archipelago. Comparison is presented for early production (upper panel), mid production (middle panel) and peak production (lowermost panel). *The observed values are presented as mean* (*solid red line*) ± *the standard error of replicate sediment traps in the rig* (*hatching*). (For interpretation of the references to colour in this figure legend, the reader is referred to the web version of this article.)

Table 5
Regression coefficients and goodness-of-fit for the correction of the model results using the linear model (Eq. (1)).

Location	Farm	Period	Scaling factor - β_1	Background deposition - B [g m^{-2} d^{-1}]	R^2
Altafjorden	Farm A1	Peak	2.423	1.85	0.67
	Farm A2	Peak	2.086	2.55	0.35
Frøya Archipelago	Farm F1	Early	0.548	5.64	0.58
		Mid	1.632	8.00	0.62
		Peak	0.621	3.25	0.80
	Farm F2	Early	0.613	0.46	0.31
		Peak	1.203	0.97	0.43

accounts of models using the constant threshold approach, especially with the 0.018 Pa critical value recommended in Cromey et al. (2002b), reporting much larger erosion of the POM than the one registered during field surveys (see Chamberlain and Stucchi, 2007; Keeley et al., 2013; Chang et al., 2014), our results seem to indicate that the use of sediment-dependent critical resuspension values can improve the depiction of the POM footprint in the salmon fish farming industry.

By comparing the bottom shear stresses calculated by the hydrodynamic model against the resuspension threshold of 0.018 Pa described in Cromey et al. (2002b), the basis for S2, we see that all farming sites in both locations can undergo resuspension episodes frequently. The situation changes when contrasting the modeled shear against the substrate-dependent thresholds identified by Carvajalino-Fernández et al. (2020) and the sediments types identified for the sites. All studied farms are located over a mixture of sediments with textures equal or coarser than sand, i.e. very few areas near the farm present cohesive beds. Under these conditions, a mean shear stress in the order of 0.1–0.3 Pa would be required to guarantee material transport, with sites like Farm F1 in Frøya Archipelago and both farms in Altafjorden falling short with respect to this condition. From this, we see that a rapid-assessment method based on the calculated bed shear stress, is a practical and simple way to identify the potential for resuspension events at a fish farming location, and therefore serves as an indicator of the complexity of the model required to simulate the spread of the particles and the extent of the POM footprint.

Results for the POM footprint analysis indicate that farms in the more dynamic location, Frøya Archipelago, are characterized by larger areas of influence and more complex POM footprints due to their shallow location and wide exposure to larger momentum stresses, caused by forces such as wind, low pressure systems and waves, when compared to the deeper, relatively sheltered Altafjorden, where a more traditional elliptical deposition pattern was dominant. Moreover, some

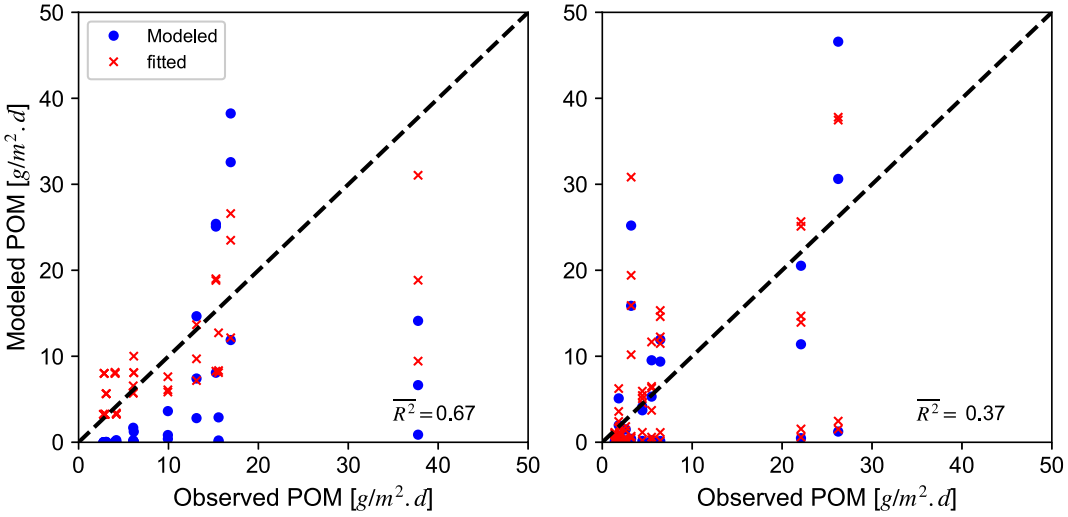

Fig. 10. Fit of model results to sediment trap POM fluxes in Frøya Archipelago using Eq. (1). Left: Farm F1, right: Farm F2. A perfect fit is represented by the black diagonal dashed line. Values for the period-averaged coefficient of determination for each farm are presented in the lower-right corner.

of our results show that POM emissions in dynamic areas can be resuspended and accumulate in quiescent areas more than 1 km from the mooring position of the farm. These relocated masses can potentially impact ecological communities far away from the area of direct influence of the farm. These so called far-field effects, are not captured by models that do not include resuspension, where particles remain at the primary (first) point of deposition (Ali et al., 2011).

One unforeseen result from this work was the specific material-relocation patterns seen under the different resuspension scenarios. A constant threshold value for resuspension generated an overall dampening of the accumulation footprint when compared to a no-resuspension case. In the former, material that was originally allocated to the direct vicinity of the farm, and therefore generating the highest deposition centers, was moved to the outskirts of the original footprint, effectively extending the low-flux areas and the span of the environmental effects of the POM. On the other hand, the limitations imposed by a substrate-dependent set of resuspension thresholds, such as those in S3, generate a more localized migration of material. In this scenario, the contribution of material to a given POM contour is provided by neighboring areas with resuspension-favoring sediments, rather than from the high accumulation zones in the direct vicinity of the farm. The difference between both scenarios becomes evident in the most dynamic sites, like the case of Farm F2 where the low resuspension threshold of S2 allows an almost complete flush of the material near the farm centers and an effective smoothing of the footprint, while the use of S3 preserves the epicenter beneath the farms at the same time that it allows for a moderate spread of the material to locations not affected in the no-resuspension scenario.

A particularly interesting case of bottom material reorganization was noticed in Altafjorden, where slightly smaller depositional footprints were obtained with the use of S3 when compared to the no-resuspension S1 alternative. We consider this to be caused by an interplay of the vertical transport scheme, the coarse nature of the sediment in the direct vicinity of the farm and the relatively weak hydrodynamic conditions in the area, causing particle accumulation in the rocky sediment patches directly beneath the farms, where the moderate bottom shears do not exceed the required critical shear stress of 0.3 Pa necessary to remobilize the material. These centers of particle accumulation were evident during video surveys in the area.

Areas exposed to POM fluxes $< 5\,g\,m^2\ d^{-1}$ constituted between 45–85% and 65–93% of the total area influenced by POM for Altafjorden and Frøya Archipelago, respectively. This indicates that the effects of low-dose, far-field exposure to POM should play a major role in the monitoring and mitigation strategies for the aquaculture sector. Moreover, this potentially important fraction of the environmental effects field can be overlooked by the use of transport models that do not include, or poorly depict, the resuspension of particles once settled upon the seafloor. The implementation of appropriate approaches to depict resuspension in aquaculture models should therefore become an area of further research and development in the future.

Even though the results for POM footprint showed particle accumulations in accordance with the existing published literature and the differences between resuspension scenarios fall in line with the expected behaviors according to the hydrodynamic and sedimentology of the sites, one major concern in the current study arises from the lack of fit between observed and simulated values along the monitored transects in the two locations. In general terms, we observe that simulations at Frøya Archipelago fit observations comparatively better than in Altafjorden. However, certain traits such as the much sharper gradients in the close vicinity of the farms are pervasive in the current version of the model and need to be addressed in future revisions.

Among the causes for the discrepancy between model and observations is the potential unsuitability of conventional sediment traps for sampling aquaculture-generated POM fluxes, as fish faeces and uneaten feed are not evenly emitted across the farm's area but have strong spatial gradients that are difficult to capture with point samplers, subjecting the measurements to strong positive and negative biases. Moreover, the inherent assumption that a sampler located 2 m above the seabed captures the resuspended material is open to debate. It is quite plausible that the resuspended particles invariably only are re-entrained to distances of < 1 m above the seabed and are therefore missed in the traps. The authors attempt to correct these issues by using a simple regression model, even if a conceptually valid approach, did not perform soundly in terms of goodness of fit and magnitude of the scaling factor (β_1). The development and use of alternate measurement methods, directly on the seabed, could improve our comprehension of model performance and of resuspension processes.

Among the most common sources of error in the hydrodynamic model are the grid resolution and turbulence parametrization, which can obscure important sub-grid scale transport processes beneath and in the near vicinity of the farm. Comparison between observed and modeled currents shows that the hydrodynamic model fails to reproduce some transient high-velocity episodes near the bottom in complex sites like Farm F1, indicating that a more accurate bathymetry and coastline, and thus a better propagation of the tidal signal and other forcings, could lead to a less abrupt decrease in modeled POM values

near the farm, more in line with the observed accumulation patterns for the area. Additionally, the current version of the model does not account for wind-generated waves and therefore doesn't include the shear stress contribution by the orbital velocities and the wave-induced momentum in coastal locations (Lee et al., 2005; Trowbridge and Lentz, 2018).

Even if the authors explored the influence of different numerical parameters and selected, on their criteria, the best candidates for this first version of the transport model, a more structure sensitivity analysis following the guidelines of e.g. Saltelli et al. (2019) is recommended in order to improve the goodness-of-fit in future model implementations. The influence of potential sources of uncertainty in the Lagrangian model, such as the particle lifespan, the temporal resolution of the feeding data, the ratio of feed to faeces conversion (Brooks and Mahnken, 2003; Reid et al., 2009; Cubillo et al., 2016), emission depth (Ali et al., 2011), particle starting point of emission (Riera et al., 2017) and wild fish consumption (Cromey et al., 2012), among others, are candidates for such further analyses.

5. Conclusions and recommendations

Even though the modest fit reported in the current version of the model against a set of deposition fluxes from sediment traps indicates that further work in terms of calibration of model parameters and validation against diverse sources of field information is needed, our results indicate that the addition of substrate-dependency into the resuspension algorithms has the potential to reduce the excess in erosion and material transport that has been previously reported in models using a single critical shear stress value for the resuspension of POM, providing trends of particle deposition more in-line with the field observations.

The observed limitations in the hydrodynamic model encourage the future use of higher horizontal resolutions (consequently better depictions of the bathymetry and the coastline), as well as the inclusion of additional processes such as surface gravity waves in order to reproduce more accurately the near-bottom, transient high-velocity events that can trigger resuspension in the areas of interest.

Future work in the topic should include the change of the constant lifespan assumption for an explicit benthic response module in the lagrangian model, as well as the use of the study of the interactions of the particles with bed-cohesiveness and additional vertical transport schemes.

Supplementary data to this article can be found online at https://doi.org/10.1016/j.marpolbul.2020.111685.

CRediT authorship contribution statement

M.A. Carvajalino-Fernández: Conceptualization, Methodology, Software, Validation, Formal analysis, Investigation, Data curation, Writing - original draft, Writing - review & editing, Visualization, Supervision. **P.N. Sævik:** Methodology, Writing - original draft, Software. **I.A. Johnsen:** Methodology, Writing - original draft, Writing - review & editing, Supervision. **J. Albretsen:** Methodology, Writing - original draft, Software. **N.B. Keeley:** Conceptualization, Investigation, Resources, Writing - original draft, Writing - review & editing, Supervision, Project administration, Funding acquisition.

Declaration of competing interest

The authors declare that they have no known competing financial interests or personal relationships that could have appeared to influence the work reported in this paper.

Acknowledgements

This work was supported by the Research Council of Norway as part of the ERA research project (Nr: 228871), also benefitting from the data collected by the Sustain-Aqua project (Nr: 267829). The high-resolution sediment maps used in this research were provided by NGU. MACF would like to thank Genoveva González-Mirelis (IMR) for providing the detailed Norwegian coastline information presented in the figures, as well as Ilker Fer (UiB/GFI) for his valuable comments on the manuscript.

References

Ådlandsvik, B., Sundby, S., 1994. Modelling the transport of cod larvae from the Lofoten area. ICES Mar. Sci. Symp. 379–392.
Albretsen, J., Sperrevik, A.K., Staalstrøm, A., Sandvik, A.D., Vikebø, F., Asplin, L., 2011. Norkyst-800 Report No. 1: User Manual and Technical Descriptions, Fisken og havet. Havforskningsinstituttet, Bergen, Norway.
Ali, A., Thiem, Ø., Berntsen, J., 2011. Numerical modelling of organic waste dispersion from fjord located fish farms. Ocean Dyn. 61, 977–989.
Bannister, R.J., Johnsen, I.A., Hansen, P.K., Kutti, T., Asplin, L., 2016. Near- and far-field dispersal modelling of organic waste from Atlantic salmon aquaculture in fjord systems. ICES Journal of Marine Science: Journal du Conseil 73, 2408–2419.
Beldring, S., Engeland, K., Roald, L.A., Sælthun, N.R., Voksø, A., 2003. Estimation of parameters in a distributed precipitation-runoff model for Norway. Hydrol. Earth Syst. Sci. 7, 304–316.
Borja, Á., Rodríguez, J.G., Black, K., Bodoy, A., Emblow, C., Fernandes, T.F., Forte, J., Karakassis, I., Muxika, I., Nickell, T.D., Papageorgiou, N., Pranovi, F., Sevastou, K., Tomassetti, P., Angel, D., 2009. Assessing the suitability of a range of benthic indices in the evaluation of environmental impact of fin and shellfish aquaculture located in sites across Europe. Aquaculture 293, 231–240.
Broch, O.J., Daae, R.L., Ellingsen, I.H., Nepstad, R., Bendiksen, E.Å., Reed, J.L., Senneset, G., 2017. Spatiotemporal dispersal and deposition of fish farm wastes: a model study from Central Norway. Front. Mar. Sci. 4.
Broch, O.J., Klebert, P., Michelsen, F.A., Alver, M.O., 2020. Multiscale modelling of cage effects on the transport of effluents from open aquaculture systems. PLoS One 15, e0228502.
Brooks, K.M., Mahnken, C.V., 2003. Interactions of Atlantic salmon in the Pacific northwest environment: II. Organic wastes. Fish. Res. 62, 255–293.
Brooks, K.M., Mahnken, C.V.W., Nash, C., 2002. Environmental effects associated with marine netpen waste with emphasis on salmon farming in the pacific northwest. In: Stickney, R.R., McVey, J.P. (Eds.), Responsible Marine Aquaculture. CABI Publishing, pp. 159–203.
Burridge, L., Weis, J.S., Cabello, F., Pizarro, J., Bostick, K., 2010. Chemical use in salmon aquaculture: a review of current practices and possible environmental effects. Aquaculture 306, 7–23.
Carvajalino-Fernández, M.A., Keeley, N.B., Fer, I., Law, B.A., Bannister, R.J., 2020. Effect of substrate type and pellet age on the resuspension of Atlantic salmon faecal material. Aquaculture Environment Interactions 12, 117–129.
Chamberlain, J., Stucchi, D., 2007. Simulating the effects of parameter uncertainty on waste model predictions of marine finfish aquaculture. Aquaculture 272, 296–311.
Chang, B.D., Page, F.H., Losier, R.J., McCurdy, E.P., 2014. Organic enrichment at salmon farms in the Bay of Fundy, Canada: DEPOMOD predictions versus observed sediment sulfide concentrations. Aquaculture Environment Interactions 5, 185–208.
Chapman, D.C., 1985. Numerical treatment of cross-shelf open boundaries in a Barotropic Coastal Ocean Model. J. Phys. Oceanogr. 15, 1060–1075.
Chen, Y.-S., Beveridge, M.C.M., Telfer, T.C., 1999. Settling rate characteristics and nutrient content of the faeces of Atlantic salmon, Salmo salar L., and the implications for modelling of solid waste dispersion. Aquac. Res. 30, 395–398.
Chen, Y.-S., Beveridge, M.C.M., Telfer, T.C., Roy, W.J., 2003. Nutrient leaching and settling rate characteristics of the faeces of Atlantic salmon (Salmo salar L.) and the implications for modelling of solid waste dispersion. J. Appl. Ichthyol. 19, 114–117.
Cromey, C.J., Nickell, T.D., Black, K.D., 2002a. DEPOMOD—modelling the deposition and biological effects of waste solids from marine cage farms. Aquaculture 214, 211–239.
Cromey, C.J., Nickell, T.D., Black, K.D., Provost, P.G., Griffiths, C.R., 2002b. Validation of a fish farm waste resuspension model by use of a particulate tracer discharged from a point source in a coastal environment. Estuaries 25, 916–929.
Cromey, C.J., Thetmeyer, H., Lampadariou, N., Black, K.D., Kögeler, J., Karakassis, I., 2012. MERAMOD: predicting the deposition and benthic impact of aquaculture in the eastern Mediterranean Sea. Aquaculture Environment Interactions 2, 157–176.
Cubillo, A.M., Ferreira, J.G., Robinson, S.M.C., Pearce, C.M., Corner, R.A., Johansen, J., 2016. Role of deposit feeders in integrated multi-trophic aquaculture — a model analysis. Aquaculture 453, 54–66.
Dean, R.J., Shimmield, T.M., Black, K.D., 2007. Copper, zinc and cadmium in marine cage fish farm sediments: an extensive survey. Environ. Pollut. 145, 84–95.
Directorate of Fisheries, 2019. Yggdrasil - Directorate of Fisheries Mapping System.
Egbert, G.D., Erofeeva, S.Y., 2002. Efficient inverse modeling of barotropic ocean tides. J. Atmos. Ocean. Technol. 19, 183–204.
Flather, R.A., 1976. A tidal model of the north-west European continental shelf. Mem. Soc. R. Sci. Liege. 10, 141–164.
Forrest, B., Keeley, N., Gillespie, P., Hopkins, G., Knight, B., Govier, D., 2007. Review of

the Ecological Effects of Marine Finfish Aquaculture: Final Report, Cawthron Report 1285. Cawthron Institute, Nelson, New Zeland, pp. 71.
Grefsrud, E., Glover, K., Grøsvik, B., Husa, V., Karlsen, Ø., Kristiansen, T., Kvamme, B., Mortensen, S., Samuelsen, O., Stien, L., Svasand, T., 2018. Risikorapport norsk fiskeoppdrett 2018, Fisken og havet.
Haidvogel, D.B., Arango, H., Budgell, W.P., Cornuelle, B.D., Curchitser, E., Di, L.E., Fennel, K., Geyer, W.R., Hermann, A.J., Lanerolle, L., Levin, J., McWilliams, J.C., Miller, A.J., Moore, A.M., Powell, T.M., Shchepetkin, A.F., Sherwood, C.R., Signell, R.P., Warner, J.C., Wilkin, J., 2008. Ocean forecasting in terrain-following coordinates: formulation and skill assessment of the Regional Ocean Modeling System. J. Comput. Phys. 227, 3595–3624.
Hall-Spencer, J., Bamber, R., 2007. Effects of salmon farming on benthic Crustacea. Ciencias Marinas 33, 353–366.
Hargrave, B.T., 2010. Empirical relationships describing benthic impacts of salmon aquaculture. Aquaculture Environment Interactions 1, 33–46.
Henry, C., Minier, J.-P., 2014. Progress in particle resuspension from rough surfaces by turbulent flows. Prog. Energy Combust. Sci. 45, 1–53.
Keeley, N.B., Forrest, B.M., Crawford, C., Macleod, C.K., 2012. Exploiting salmon farm benthic enrichment gradients to evaluate the regional performance of biotic indices and environmental indicators. Ecol. Indic. 23, 453–466.
Keeley, N.B., Cromey, C.J., Goodwin, E.O., Gibbs, M.T., Macleod, C.M., 2013. Predictive depositional modelling (DEPOMOD) of the interactive effect of current flow and resuspension on ecological impacts beneath salmon farms. Aquaculture Environment Interactions 3, 275–291.
Keeley, N., Valdemarsen, T., Woodcock, S., Holmer, M., Husa, V., Bannister, R., 2019. Resilience of dynamic coastal benthic ecosystems in response to large-scale finfish farming. Aquaculture Environment Interactions 11, 161–179.
Keeley, N., Valdemarsen, T., Strohmeier, T., Pochon, X., Dahlgren, T., Bannister, R., 2020. Mixed-habitat assimilation of organic waste in coastal environments - it's all about synergy!. Sci. Total Environ. 699, 134281.
Kutti, T., Ervik, A., Hansen, P.K., 2007. Effects of organic effluents from a salmon farm on a fjord system. I. Vertical export and dispersal processes. Aquaculture 262, 367–381.
Law, B.A., Hill, P.S., Milligan, T.G., Zions, V., 2016. Erodibility of aquaculture waste from different bottom substrates. Aquaculture Environment Interactions 8, 575–584.
Lee, C., Schwab, D.J., Hawley, N., 2005. Sensitivity analysis of sediment resuspension parameters in coastal area of southern Lake Michigan. Journal of Geophysical Research: Oceans 110.
Lien, V.S., Gusdal, Y., Vikebø, F.B., 2014. Along-shelf hydrographic anomalies in the Nordic Seas (1960–2011): locally generated or advective signals? Ocean Dyn. 64, 1047–1059.
Lynch, D.R., Greenberg, D.A., Bilgili, A., McGillicuddy, J.D.J., Manning, J.P., Aretxabaleta, A.L., 2015. Particles in the Coastal Ocean: Theory and Applications. Cambridge University Press, New York, NY, USA.
Macleod, C., Eriksen, R., Simpson, S.L., Davey, A., Ross, J., 2014. Assessment of the Environmental Impacts and Sediment Remediation Potential Associated With Copper Contamination From Antifouling Paint (and Associated Recommendations for Management). Fisheries Research and Development Corporation, Australia, pp. 76.
Marchesiello, P., McWilliams, J.C., Shchepetkin, A., 2001. Open boundary conditions for long-term integration of regional oceanic models. Ocean Modelling 3, 1–20.
Martin, J., McCutcheon, S., 1999. Hydrodynamics and Transport for Water Quality Modelling. CRC Press, Boca Raton.
Müller, M., Homleid, M., Ivarsson, K.-I., Køltzow, M.A.Ø., Lindskog, M., Midtbø, K.H., Andrae, U., Aspelien, T., Berggren, L., Bjørge, D., Dahlgren, P., Kristiansen, J., Randriamampianina, R., Ridal, M., Vignes, O., 2017. AROME-MetCoOp: a nordic convective-scale operational weather prediction model. Weather and Forecasting 32, 609–627.
Nærings- og fiskeridepartementet, 2017. Forskrift om produksjonsområder for akvakultur av matfisk i sjø av laks, ørret og regnbueørret (produksjonsområdeforskriften), in: fiskeridepartementet, N.-o. (Ed.), FOR-2017-01-16-61, Norway.
Nordam, T., Nepstad, R., Litzler, E., Rohrs, J., 2019. On the use of random walk schemes in oil spill modelling. Mar Pollut Bull 146, 631–638.
Okubo, A., Levin, S., 2001. Diffusion and Ecological Problems: Modern Perspectives, 2nd ed. Springer-Verlag New York.
Reid, G.K., Liutkus, M., Robinson, S.M.C., Chopin, T.R., Blair, T., Lander, T., Mullen, J., Page, F., Moccia, R.D., 2009. A review of the biophysical properties of salmonid faeces: implications for aquaculture waste dispersal models and integrated multi-trophic aquaculture. Aquaculture Research 40, 257–273.
Riera, R., Pérez, Ó., Cromey, C., Rodríguez, M., Ramos, E., Álvarez, O., Domínguez, J., Monterroso, Ó., Tuya, F., 2017. MACAROMOD: a tool to model particulate waste dispersion and benthic impact from offshore sea-cage aquaculture in the Macaronesian region. Ecological Modelling 361, 122–134.
Saltelli, A., Aleksankina, K., Becker, W., Fennell, P., Ferretti, F., Holst, N., Li, S., Wu, Q., 2019. Why so many published sensitivity analyses are false: a systematic review of sensitivity analysis practices. Environmental Modelling & Software 114, 29–39.
Sarà, G., Scilipoti, D., Mazzola, A., Modica, A., 2004. Effects of fish farming waste to sedimentary and particulate organic matter in a southern Mediterranean area (Gulf of Castellammare, Sicily): a multiple stable isotope study (δ13C and δ15N). Aquaculture 234, 199–213.
Scheffer, M., Baveco, J.M., DeAngelis, D.L., Rose, K.A., van Nes, E.H., 1995. Super-individuals a simple solution for modelling large populations on an individual basis. Ecological Modelling 80, 161–170.
Shchepetkin, A.F., McWilliams, J.C., 2005. The regional oceanic modeling system (ROMS): a split-explicit, free-surface, topography-following-coordinate oceanic model. Ocean Modelling 9, 347–404.
Skamarock, W., Klemp, J., Dudhia, J., Gill, D., Barker, D., Duda, M., Huang, X.Y., Wang, W., 2008. A Description of the Advanced Research WRF Version 3. NCAR Technical Notes. National Center for Atmospheric Research, Boulder, Colorado (USA).
Skarðhamar, J., Albretsen, J., Sandvik, A.D., Lien, V.S., Myksvoll, M.S., Johnsen, I.A., Asplin, L., Ådlandsvik, B., Halttunen, E., Bjørn, P.A., 2018. Modelled salmon lice dispersion and infestation patterns in a sub-arctic fjord. ICES Journal of Marine Science 75, 1733–1747.
Taranger, G.L., Karlsen, O., Bannister, R.J., Glover, K.A., Husa, V., Karlsbakk, E., Kvamme, B.O., Boxaspen, K.K., Bjorn, P.A., Finstad, B., Madhun, A.S., Morton, H.C., Svasand, T., 2014. Risk assessment of the environmental impact of Norwegian Atlantic salmon farming. ICES Journal of Marine Science 72, 997–1021.
Traugott, H., Liberzon, A., 2017. Experimental study of forces on freely moving spherical particles during resuspension into turbulent flow. International Journal of Multiphase Flow 88, 167–178.
Trowbridge, J.H., Lentz, S.J., 2018. The bottom boundary layer. Annual Review of Marine Science 10, 397–420.
Umlauf, L., Burchard, H., 2003. A generic length-scale equation for geophysical turbulence models. Journal of Marine Research 61, 235–265.
Visser, A.W., 1997. Using random walk models to simulate the vertical distribution of particles in a turbulent water column. Marine Ecology Progress Series 158, 275–281.
Warner, J.C., Sherwood, C.R., Signell, R.P., Harris, C.K., Arango, H.G., 2008. Development of a three-dimensional, regional, coupled wave, current, and sediment-transport model. Computers & Geosciences 34, 1284–1306.
Wassmann, P., Svendsen, H., Keck, A., Reigstad, M., 1996. Selected aspects of the physical oceanography and particle fluxes in fjords of northern Norway. Journal of Marine Systems 8, 53–71.
Weise, A.M., Cromey, C.J., Callier, M.D., Archambault, P., Chamberlain, J., McKindsey, C.W., 2009. Shellfish-DEPOMOD: Modelling the biodeposition from suspended shellfish aquaculture and assessing benthic effects. Aquaculture 288, 239–253.
Woodcock, S.H., Strohmeier, T., Strand, Ø., Olsen, S.A., Bannister, R.J., 2018. Mobile epibenthic fauna consume organic waste from coastal fin-fish aquaculture. Marine Environmental Research 137, 16–23.
Woodcock, S.H., Meier, S., Keeley, N.B., Bannister, R.J., 2019. Fate and longevity of terrestrial fatty acids from caged fin-fish aquaculture in dynamic coastal marine systems. Ecological Indicators 103, 43–54.